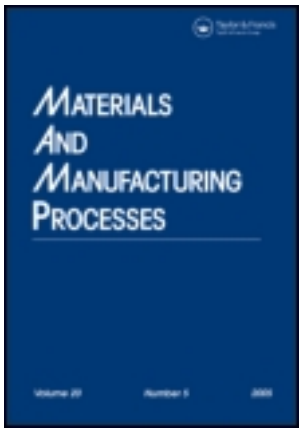

Materials and Manufacturing Processes
Publication details, including instructions for authors and subscription information:
http://www.tandfonline.com/loi/lmmp20

FABRICATION AND CHARACTERIZATION OF Cu-SiC_p COMPOSITES FOR ELECTRICAL DISCHARGE MACHINING APPLICATIONS

Kuen-Ming Shu [a] & G. C. Tu [a]
[a] Department of Materials Science and Engineering , National Chiao-Tung University 1001 , Ta Hsueh Road, Hsinchu, 30050, Taiwan
Published online: 07 Feb 2007.

To cite this article: Kuen-Ming Shu & G. C. Tu (2001) FABRICATION AND CHARACTERIZATION OF Cu-SiC_p COMPOSITES FOR ELECTRICAL DISCHARGE MACHINING APPLICATIONS, Materials and Manufacturing Processes, 16:4, 483-502, DOI: 10.1081/AMP-100108522

To link to this article: http://dx.doi.org/10.1081/AMP-100108522

MATERIALS AND MANUFACTURING PROCESSES, 16(4), 483–502 (2001)

FABRICATION AND CHARACTERIZATION OF Cu–SiC_p COMPOSITES FOR ELECTRICAL DISCHARGE MACHINING APPLICATIONS

Kuen-Ming Shu* and G. C. Tu

Department of Materials Science and Engineering, National Chiao-Tung University 1001, Ta Hsueh Road, Hsinchu 30050, Taiwan

ABSTRACT

Cu–SiC_p composites made by the powder metallurgy method were investigated. To avoid the adverse effect of Cu–SiC_p reaction, sintering was controlled at a reaction temperature less than 1032 K. Electroless plating was employed to deposit a copper film on SiC_p powder before mixing with Cu powder in order to improve the bonding status between Cu and SiC particles during sintering. It was found that a continuous copper film could be deposited on SiC_p by electroless copper plating, and a uniform distribution of SiC_p in Cu matrix could be achieved after the sintering and extrusion process. The mechanical properties of Cu–SiC_p composites with SiC_p contents from 0.6 to 10 wt% were improved evidently, whereas electrical properties remained almost unchanged as compared with that of the pure copper counterpart. In the electrical discharge machining (EDM) test, the as-formed composite electrodes exhibited a character of lower electrode wear ratio, justifying its usage. The optimum conditions for EDM were Cu–2 wt% SiC_p composite electrode operating with a pulse time of 150 μsec.

Key Words: Copper-based composite; Density; Electrical discharge machining; Electrical resistivity; Electrode wear ratio; Electroless copper plating; Fracture surface; Hardness; Material removal rate; Metal matrix composite; Porosity; Powder metallurgy; Silicon carbide; Tensile strength; Thermal expansion coefficient.

* Corresponding author. E-mail: KMShu@sunws.nhit.edu.tw

1.0 INTRODUCTION

To machine hard material, such as carbide and molding steel, the electrical discharge machining (EDM) process is often used. In the mold manufacturing industry, the EDM is often used despite its slow machining rate. EDM research has concentrated on achieving faster and more efficient metal removal rate coupled with reducing tool wear and maintaining reasonable accuracy. Recently, tool electrode fabrication became the focus of many studies in EDM technology (1,2), paralleling the development of EDM machine parts such as high-performance generators and adaptive control mechanisms (3,4). The majority of work has been done using a mechanically formed tool electrode; however, because of its economical and technological disadvantages, the EDM user is compelled to search for alternative tooling (5).

Copper and copper-based alloys are widely used in the electrical industry. The addition of ceramic reinforcements such as carbides and oxides to form metal matrix composites (MMCs) enhances the properties such as elastic modulus, strength, wear resistance, and high-temperature durability (6,7). These attractive properties are expected to widen the application of copper composite materials.

At temperatures in excess of 773 K, copper undergoes thermal softening. As a result, a substantial deterioration in its tensile strength and creep resistance takes place (8). There is clearly a need for a copper conductor with electrical conductivity above 80% International Annealed Copper Standard (IACS) and capable of operating above 773 K for a variety of uses, including electrical and resistance welding electrodes (9). Thus, the research in fabricating copper-based composite materials is ongoing, including $Cu–Al_2O_3$, $Cu–Zr–Al_2O_3$, $Cu–TiO_2$, $Cu–Si_3N_4$, $Cu–B_4C$, and Cu–SiC (10–14). Methods for fabricating these composite materials include casting, coprecipitation, internal oxidation, and powder metallurgy (15–20).

Owing to the poor wetting ability and dispersion between copper and reinforcements, the casting methods are impractical. The methods of coprecipitation and internal oxidation are not suitable for mass production, so the powder metallurgy method is the preferred choice.

A nonhomogeneous distribution also occurs when the ceramic powders are incorporated with copper by powder metallurgy, especially when the reinforcements are extremely fine, and when a V-blender or tumble mixer is used (21). The resulting agglomerates lead to unacceptable porosity levels, nonhomogeneous microstructures, and poor interfacial bonding.

A copper film coated on ceramic powder by electroless plating can improve the bonding between ceramic powder and copper powder. The high strength and high electrical conductivity of a copper-based composite can be obtained after sintering when the coated ceramic powder is mixed with copper powder by the mechanical alloying method.

The stability of SiC particles in copper was evaluated by Groza and Gibeling

(22). Their results show that the SiC particle becomes thermodynamically unstable at 1300 K. The result is reasonable because in the Cu–Si–C phase diagram, reported by Warren and Anderson (23), there exists a reacted liquid phase with copper and SiC at 1173 K. Although SiC fiber is reckoned to be decomposed by molten copper at 1356 K and results in the formation of a low-temperature eutectic product according to the Cu–Si–C phase diagram at 1173 K, no reaction was observed between the copper matrix and SiC fiber after a holding time of 3 hr at the melting point of copper (1356 K). However, Qin and Derby (24) showed experimentally that a solid-state reaction occurs between SiC plate and copper deposit at 1173 K. At this temperature, the reaction product of Cu_3Si becomes liquid (melting point 1132 K). Although Groza and Gibeling suggested that the SiC particle is useless for dispersion-strengthened copper alloy (22), for EDM application, the physical properties are as important as the electrical properties of the electrode. Decreasing the harmful factor of physical properties and retaining the virtuous factor of electrical properties enable fabrication of an optimum copper-based EDM electrode.

This paper presents the research aimed at the production of Cu–SiC_p composites by powder metallurgy without solid reaction. This composite is expected to possess high density, high electrical conductivity, and low coefficient of thermal expansion (CTE), and is suitable for EDM usage. The influence of the weight fraction of SiC_p on the mechanical properties was examined. The microstructure and fracture surfaces of composites were observed by optical microscope (OM) and scanning electron microscope (SEM). The two factors of material removal rate and electrode wear ratio on EDM were evaluated to investigate the feasibility of the fabricated Cu–SiC_p electrode material.

2.0 EXPERIMENTAL PROCEDURE

The metal matrix powder used in this experiment was electrolytic copper powder (99.7% pure). The particle morphology was dendritic and average size was 30 μm. Figure 1 shows the SiC_p powder (average powder size is 4 μm) used as reinforcements.

To obtain optimal bonding between SiC_p and Cu particles and a completely continuous copper film on SiC_p, the following steps were followed.

2.1 Surface Treatment

Surface cleaning of SiC_p was accomplished by immersing it in acetone under ultrasonic vibration for 30 min. After rinsing well with deionized water, and heating at 873 K for 3 hr in an air-drying oven, the SiC was slightly ground to break agglomerated particles.

Marcel Dekker, Inc.
270 Madison Avenue, New York, New York 10016

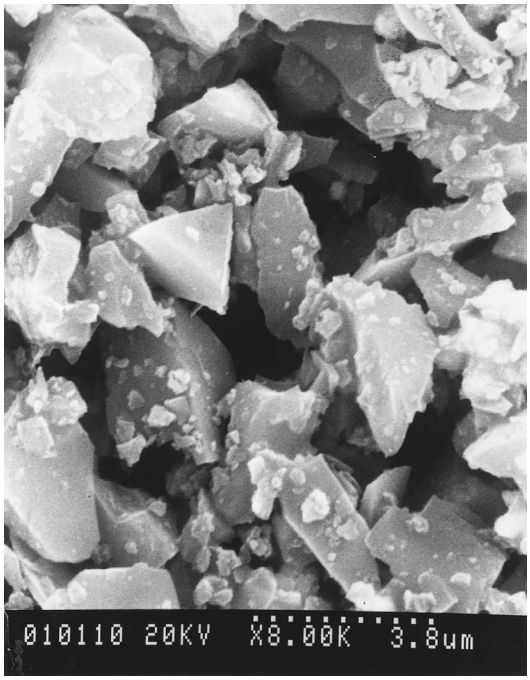

Figure 1. SEM micrograph of SiC_p.

2.2 Sensitization and Activation

The cleaned SiC_p samples were sensitized in a solution containing stanous chloride ($SnCl_2 \cdot 2H_2O$) and hydrochloric acid (HCl) for 1 hr and then activated in a solution containing palladium chloride ($PdCl_2$) and hydrochloric acid for a few hours.

2.3 Electroless Copper Process

Before the procedure of mixing, continuous stirring, and rinsing, the cleaned SiC_p was put into $CuSO_4 \cdot 5H_2O$ (20 g/l) and $KNaC_4H_4O_6$ (50 g/l) individually, shaken by ultrasound, and then HCOH (36%) and NaOH were added. The pH value of the solution was adjusted by adding NaOH until the pH value approached 13, then the copper film was created. The thick film was obtained by later immersing it in Fehling solution. The components of Fehling solution are as follows: $CuSO_4 \cdot 5H_2O$ (10 g/l); $KNaC_4H_4O_6$ (25 g/l); HCOH (50 ml/l); and NaOH (7 g/l).

The mixture of the constituent powders with the preselected SiC percentages (0.6, 2, 4, 6, 8, and 10 wt%) was milled with aluminum balls as the grinding medium in Ar atmosphere, and cold formed by pressing the powders with a unit pressure of 450 MPa.

Table 1. Specimen Classification

Specimen ID	Composition of Compact (wt% SiC)	Copper Coating	Extrusion
C1	0.6, 2, 4, 6, 8, 10	Yes	Yes
C2	0.6, 2, 4, 6, 8, 10	Yes	No
R1	0.6, 2, 4, 6, 8, 10	No	Yes
R2	0.6, 2, 4, 6, 8, 10	No	No

A series of compacts was heated to 1073 K for 4 hr in hydrogen, and then extruded at 973 K by an indirect extrusion method with a 15:1 extrusion ratio. The specimen classifications are summarized in Table 1.

Composite testing involved measurements of the density, hardness, ultimate stress, volume electrical resistivity, and CTE. The density of the Cu–SiC_p composites was measured by using the buoyancy (Archimedes) method. The hardness measurement was performed with a Rockwell hardness tester. Uniaxial tensile testing with a constant cross-head speed of 1.0 mm/min was carried out on a Instron testing machine at room temperature; specimens were machined according to ASTM E8 standard. The four-probe method was used for measuring the electrical resistivity.

The CTE value was obtained using a thermal mechanical analyzer. The products were characterized by means of X-ray diffraction as well as OM, SEM, and transmission electron microscopy (TEM). The particle diameter was measured using a Honeywell UPA particle size analyzer. EDM testing was performed on a Charmer CM30A EDM machine.

3.0 RESULTS AND DISCUSSION

3.1 Change of Powder Particles by Electroless Plating and Milling

Electroless Cu-coated SiC_p samples are shown in Figure 2. The coated copper film is homogenous and continuous. The thickness of the Cu film given in Table 2 was found to be about 0.6 μm.

Figure 3 shows the X-ray diffraction (XRD) patterns of the treated and the copper-coated SiC_p particles. Figure 3a shows the XRD pattern of SiC_p (which was obtained before adding HCOH and NaOH); the copper tartrate (CuT) and SiC peaks were detected, and no detectable peak appeared for palladium. This is because the concentration of palladium was extremely low and palladium spreads over the surface at the atomic level. After coating, as shown in Fig. 3b, three new peaks appeared at $2\theta = 43.2$, 50.6, and 74.5°. These results indicate that the Cu was coated on the SiC particle.

Figure 4 shows the change in powder–particle morphology of 2 wt% SiC–Cu powder following 8 hr of ball milling. The powder particles underwent re-

Marcel Dekker, Inc.
270 Madison Avenue, New York, New York 10016

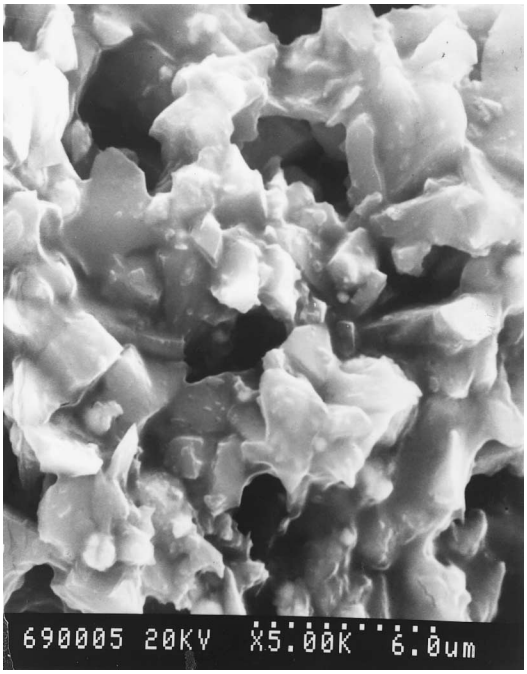

Figure 2. SEM micrograph of SiC_p coated with Cu.

Table 2. Particle Size of SiC_p Determined Using Honeywell UPA

Percentile	Uncoated SiC_p (μm) A	Coated SiC_p (μm) B	Thickness of Cu Film (μm) (B-A)/2
10%	3.442	4.749	0.6535
20%	3.650	4.936	0.643
30%	3.829	5.099	0.635
40%	3.991	5.256	0.6325
50%	4.148	5.413	0.6325
60%	4.321	5.579	0.629
70%	4.494	5.754	0.630
80%	4.732	5.956	0.612
90%	5.129	6.190	0.5305
95%	5.478	6.342	0.432

MARCEL DEKKER, INC.
270 Madison Avenue, New York, New York 10016

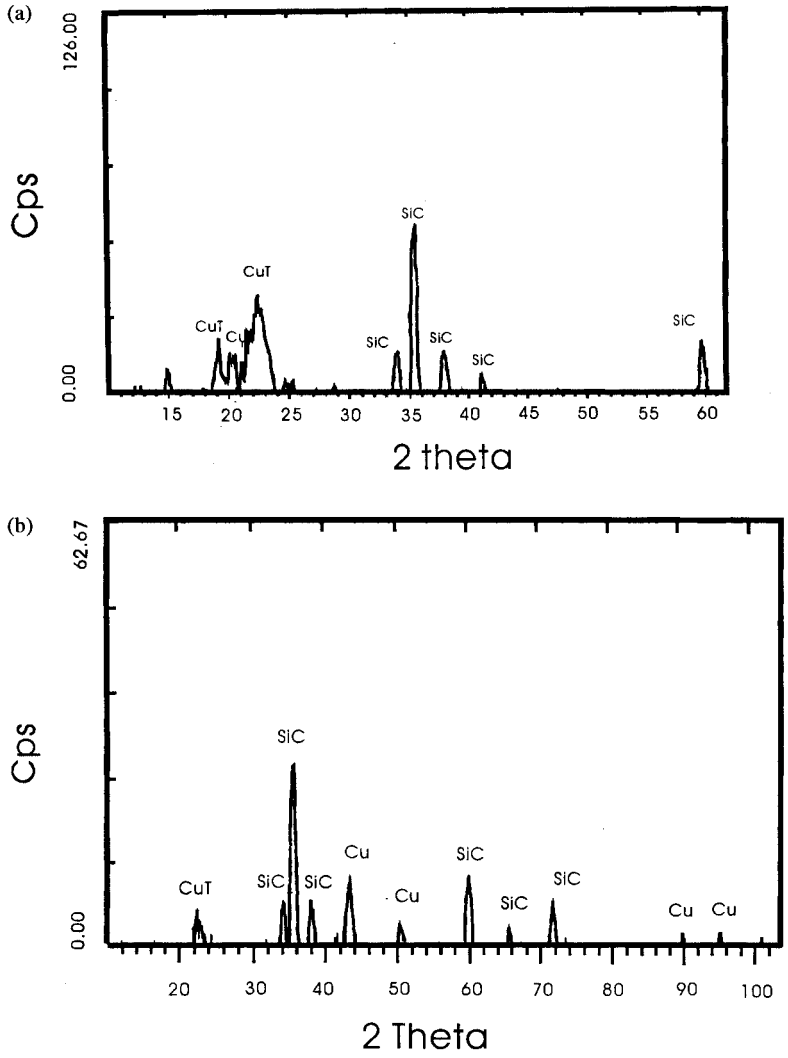

Figure 3. The XRD patterns of the particles. (a) SiC$_p$ activated with palladium; (b) SiC$_p$ plated with copper.

peated flattening and fracturing as a result of the collisions of the milling balls in the mechanical milling mixture, and consequently became fine powder of flattened particles which look different from the original dendritic shape.

3.2 Density

The true densities obtained by Archimedes' law and the theoretical values are listed in Table 3 for comparison. It was observed that the density of the com-

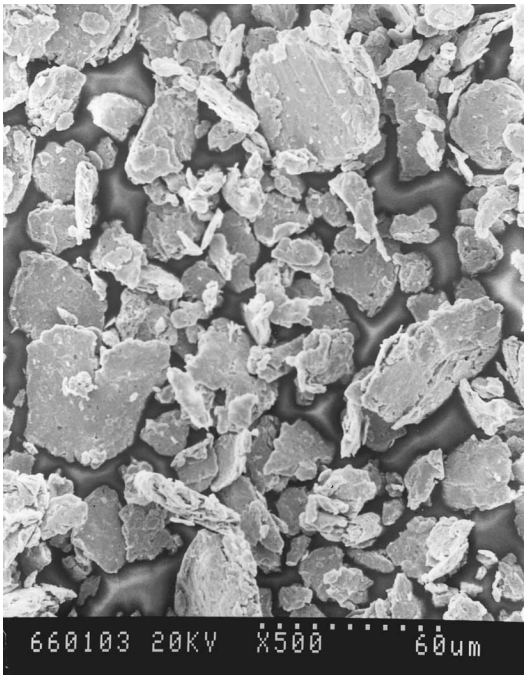

Figure 4. The change in powder–particle morphology of 2 wt% SiC_p–Cu for plated samples after 8 hr of ball milling.

posite with electroless copper-plated SiC_p for all wt% SiC_p is a little higher than that without the coating.

The porosity can be determined by the following equation (25):

$$f_p = 1 - \rho/\rho_0 \tag{1}$$

where f_p is the pore volume fraction, ρ is the measured density, ρ_0 is the theoretical density.

Table 3. Sample Density

Copper with SiCp wt%	Measured Density				Theoretical Density
	Before Extrusion		After Extrusion		
	Coated	Uncoated	Coated	Uncoated	
0%	7.67		8.61		8.96
0.6%	7.56	7.45	8.60	8.40	8.86
2%	7.37	7.25	8.36	8.19	8.65
4%	7.12	6.88	7.95	7.89	8.36
6%	6.87	6.58	7.70	7.59	8.09
8%	6.50	6.24	7.45	7.24	7.84
10%	6.21	6.01	7.19	7.02	7.60

MARCEL DEKKER, INC.
270 Madison Avenue, New York, New York 10016

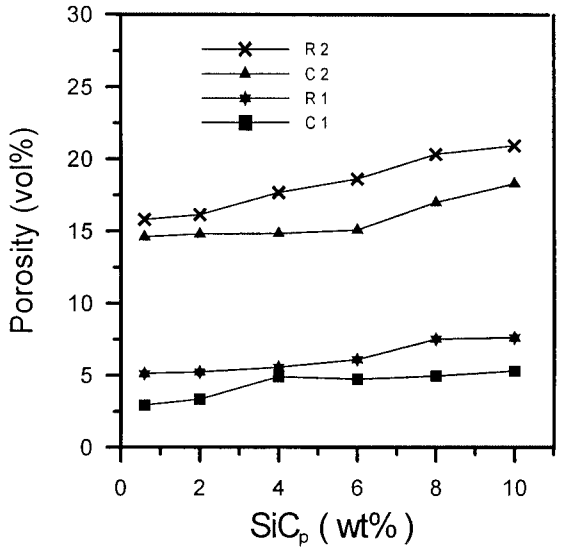

Figure 5. Variation of porosity with SiC_p contents for the Cu–SiC_p composite.

Figure 5 reveals that, compared to the composites made by the extrusion process, all of the composites made by the as-sintering process had relatively high porosity. For the composites made by extrusion, although the porosity increased with increasing SiC_p content, the porosity remained comparatively low.

Figure 6 shows SEM micrographs of polished samples of composites containing 2 wt% SiC_p. The composite made by the as-sintering method (Fig. 6a) contained a large amount of pores, with most of the pores ranging in size from 2 to 40 μm. Some large pores were observed to have flat shapes. However, no large pore was observed in the composite made by the extrusion method (Fig. 6b). In Figure 5, it also can be observed that the porosities of C1 and C2 specimens are slightly lower than those of R1 and R2 specimens individually; this indicated that the density of composites can be improved to a certain extent by coating a copper film on SiC_p. This is presumably caused by better sintering ability between coated SiC–Cu compared to SiC–Cu particles. A hot extrusion process can improve the density of the composites up to 95% of the theoretical density value. As shown in Figure 5, the porosity of the coated 2 wt% SiCp composite significantly decreased following the extrusion process.

3.3 Tensile Strength

The tensile properties of various Cu–SiC_p specimens are given in Table 4. It shows that apparently the tensile properties have been significantly improved through hot extrusion. This is probably because of reduction in the amount and size of the porosity after hot extrusion, interfacial bonding enhancement between

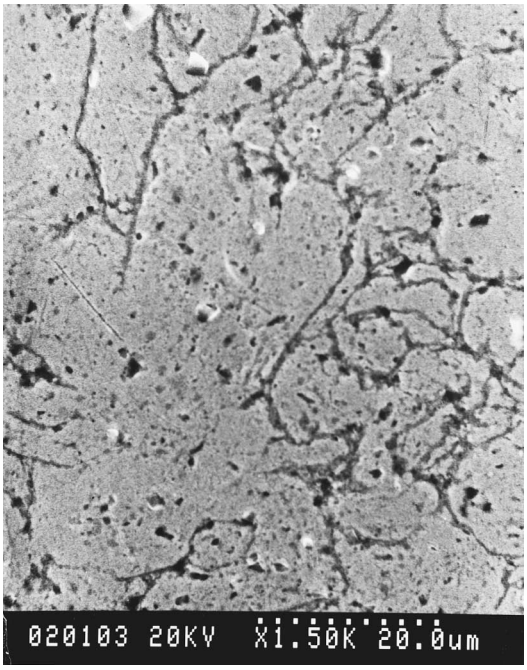

(a)

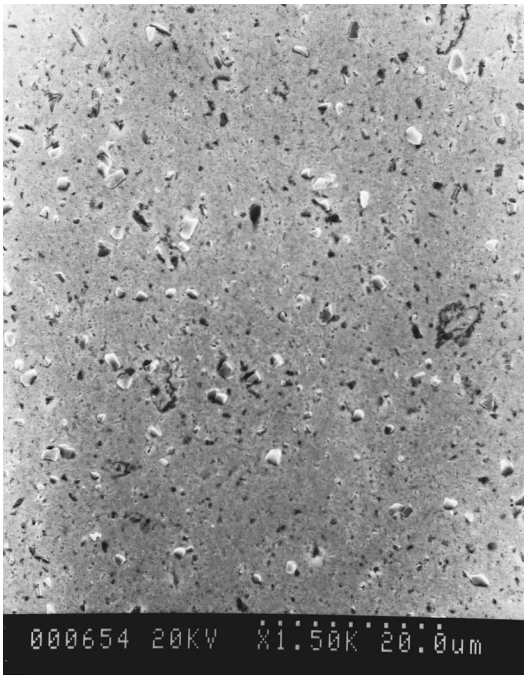

(b)

Figure 6. SEM micrographs of the 2 wt% SiC_p–Cu composites (a) as sintering, and (b) extruded.

MARCEL DEKKER, INC.
270 Madison Avenue, New York, New York 10016

Table 4. Tensile Test Results

SiCp Contents	Specimen	Modulus (Gpa)	0.2% YS (Mpa)	UTS (Mpa)	Elongation (%)
0.6%	C1	81	159	253	5.32
	C2	77	151	249	5.28
	R1	71	128	214	5.30
	R2	71	127	208	5.02
2%	C1	83	178	292	4.38
	C2	81	166	268	4.17
	R1	76	125	212	4.32
	R2	72	117	192	3.98
4%	C1	84	175	277	2.41
	C2	80	156	260	2.24
	R1	78	113	195	2.31
	R2	77	96	177	2.18
6%	C1	85	138	243	1.86
	C2	82	142	237	1.79
	R1	81	103	182	1.84
	R2	80	93	173	1.76
8%	C1	86	132	229	1.53
	C2	84	130	214	1.31
	R1	83	104	168	1.32
	R2	79	101	158	1.29
10%	C1	86	124	210	1.44
	C2	85	119	202	1.41
	R1	84	90	155	1.42
	R2	81	87	150	1.28

SiC and the matrix, grain reinforcement of Cu matrix, and a more homogeneous distribution of SiC after hot extrusion. The wt% of SiC_p and the electroless plating process were found to tremendously influence the tensile property of copper matrix composite. Figure 7 demonstrates that ultimate stress decreases with an increasing amount of uncoated SiC_p. There is a maximum value of ultimate stress at 2 wt% if the SiC_p particles are electroless plated with copper. This phenomenon is caused by particle reinforcement. The strength of composite decreases if the SiC_p is increased, because more defects are produced. The tensile strength of composites with uncoated SiC_p is lower than the composites with electroless-plated SiC_p. The strength of the composite is reduced by the presence of SiC_p owing to the poor bonding between the uncoated SiC_p and copper.

3.4 Hardness

Figure 8 shows the change in the Rockwell hardness number of Cu–SiC_p composites for various SiC_p wt% made by various methods. The hardness value increases with increasing SiC_p wt%. Generally, the hardness of material increases

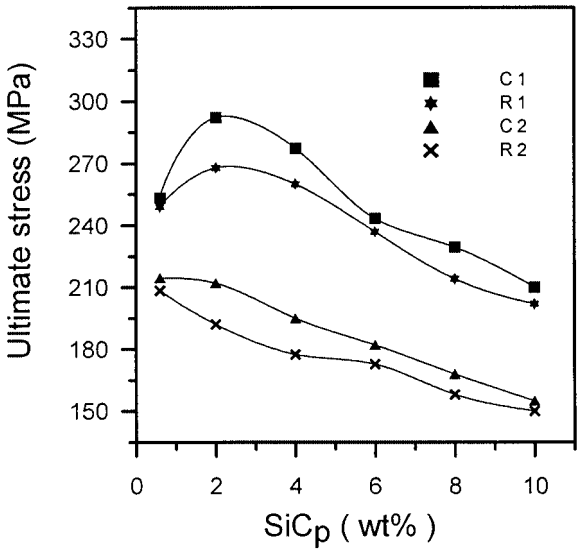

Figure 7. The ultimate stress in Cu–SiC_p composites.

with increase of material strength. However, in the present work, the strength decreased with increasing SiC_p wt% (Fig. 7). As can be seen in Figure 5, the porosity increases with increasing SiC_p wt%; this is responsible for the corresponding decreasing stress and increasing hardness tendencies (Figs. 7 and 8, respectively). The former tendency has been explained in section 3.3. The latter

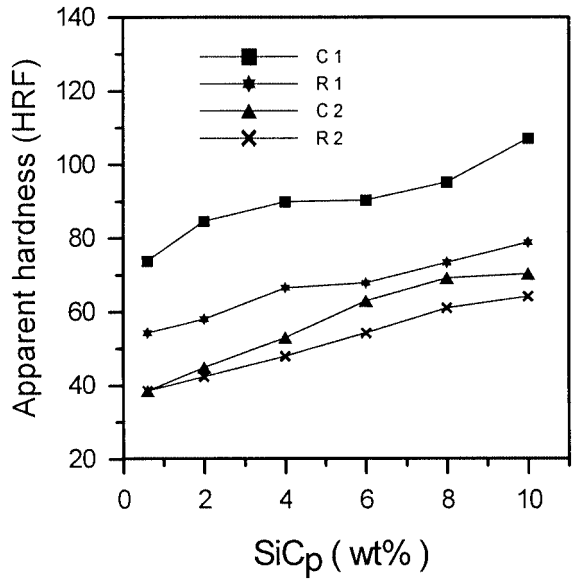

Figure 8. The Rockwell hardness number of Cu–SiC_p composite.

MARCEL DEKKER, INC.
270 Madison Avenue, New York, New York 10016

increasing hardness tendency is qualitatively explained as follows: the Cu–SiC_p hardness is probably determined by the composite effect of porosity and SiC particles. It is apparent that the Cu–SiC interface increases with increasing SiC_p wt%, thus hindering more seriously the Cu slipping and resulting in increased hardness. In this work, the pore sizes were only about one-half to one-third of SiC_p sizes (Fig. 6) and the porosity increased only mildly with SiC_p (Fig. 5). Therefore, the effect of porosity on hardness would appear much less important than the dominant effect of Cu/SiC interface (i.e., the inherent high SiC hardness).

The promoted bonding between SiC_p and Cu by copper-coating method restrains more effectively elastic and plastic deformation of the composites, leading to higher hardness. Much lower porosity can be achieved through the extrusion process, rendering higher composite hardness.

3.5 Fracture Surface

SEM micrographs of the fracture surfaces of the composites with 0.6 wt% uncoated SiC_p content having poor interface bonding between the matrix and the particle is shown in Figure 9a. SiC_p shows relatively flat surfaces, and a sample with 2 wt% coated SiC_p content (where the copper film can be seen on the surface of SiC_p) is shown in Figure 9b. In both samples, fracture appears to initiate at the SiC_p particles, with the fracture surfaces characterized by the presence of large microvoids with SiC_p particles at the center of each dimple. The crack may propagate along the interface between SiC_p particles and matrix, and within SiC_p particles. In addition to the normal ductile dimple fracture of the matrix, there are two types of fracture behavior involved with SiC_p particulate: fracture of SiC_p and Cu–SiC_p interface decohesion. In Figure 9a, the fracture surface shows the presence of decohesion at the Cu–SiC_p interface. However, the occurrence of SiC_p fracture was observed in Figure 9b, and this indicates that there was load transfer from the matrix to the SiC_p particulate.

3.6 Electrical Resistivity

The electrical resistivity of composites depends on the size and number of microweldments developed between particles during sintering. Figure 10 indicates that the electrical resistivity is increased with a higher SiC_p content.

The effective electrical resistivity σ_{eff} of two-phase composite materials can be determined by the simple rule of mixture (ROM) when the electrical resistivity of both phases are comparable, i.e., $\sigma_1 \sim \sigma_2$ (26), and

$$\sigma_{eff} = f_1 \times \sigma_1 + f_2 \sigma_2 \tag{2}$$

where f_i is the volume fraction and σ_i is the electrical resistivity of phase i.

Marcel Dekker, Inc.
270 Madison Avenue, New York, New York 10016

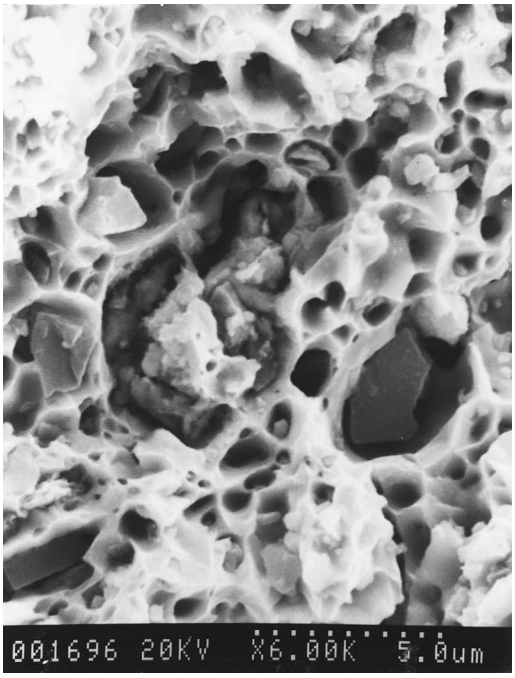

(a)

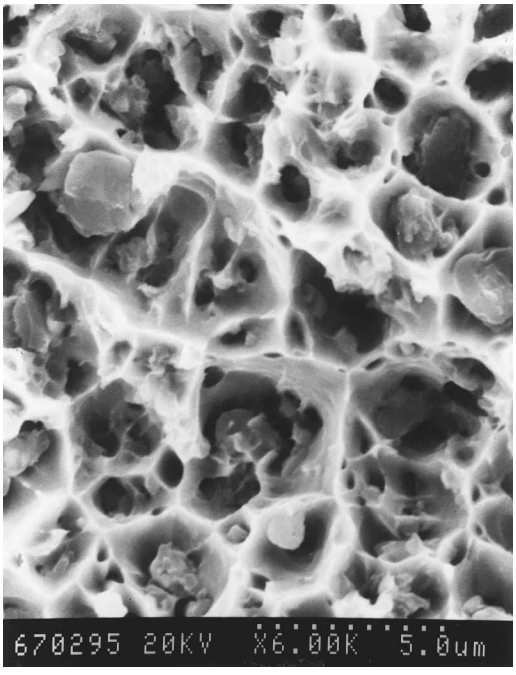

(b)

Figure 9. SEM micrographs of the fracture surface of composites in (a) 0.6% uncoated SiC_p, and (b) 2 wt% coated SiC_p.

MARCEL DEKKER, INC.
270 Madison Avenue, New York, New York 10016

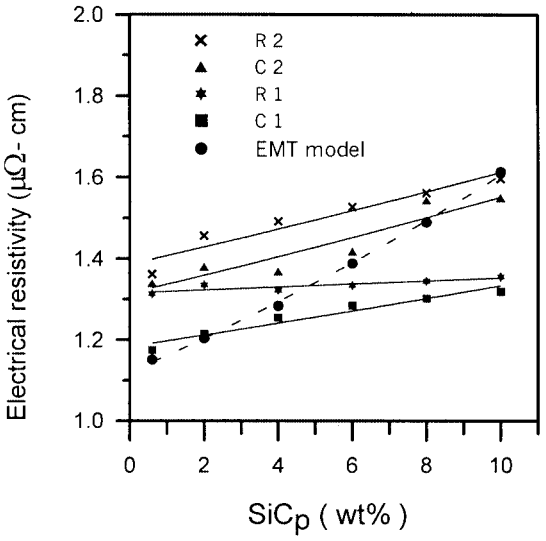

Figure 10. Measured and predicted electrical resistivity of Cu–SiC$_p$ composites.

The σ_{eff} value is 166,001 μΩ-cm if the ROM model is used to calculate the effective electrical resistivity of composite with 0.6 wt% of SiC$_p$ content, and a large discrepancy from experiment data was found.

When the difference between electrical resistivity of constituent phases is increased, the dependence of the effective resistivity on the volume fraction becomes nonlinear, and the electrical resistivity can be represented by the effective medium theory (EMT). EMT considers a spherical entity consisting of a single phase embedded in the surrounding effective medium, with the following relation given in reference 27:

$$f_1 \times \frac{\sigma_1 - \sigma_{eff}}{\sigma_1 + 2\sigma_{eff}} + f_2 \times \frac{\sigma_2 - \sigma_{eff}}{\sigma_2 + 2\sigma_{eff}} = 0 \tag{3}$$

where the surface electrical resistivity of copper and SiC$_p$ are 1.130 and 1.0×10^7 μΩ cm, respectively. The electrical resistivity of the copper composite calculated by the above model gives close results to the experimental data shown in Figure 10.

3.7 CTE

Because the CTEs for Cu and SiC$_p$ are 16.9×10^{-6} K^{-1} (293–573 K) and 5.0×10^{-6} K^{-1}, respectively (28,29), it is expected that the CTE of the composite would be lowered with the addition of SiC$_p$. The CTE of a particle-reinforced composite is often estimated by three popular models (30), for which the ROM model is often considered inappropriate because it does not take into account

the microstructure and strain interactions. The Turner's model (31), considering uniform hydrostatic stresses exit in the phases, predicts the CTE of a composite by

$$\alpha_c = \frac{\alpha_p f_p k_p + \alpha_m f_m k_m}{f_p k_p + f_m k_m} \tag{4}$$

where α_c, α_p, and α_m are the CTEs of composites, reinforcements, and matrix, respectively; k_m is the bulk modulus of matrix; and the Kerner's model (32) accounts for both the shear and isostatic stress developed in the component phases and determines the composite CTE by

$$\alpha_c = \alpha_p f_p + \alpha_m f_m + (\alpha_p - \alpha_m) f_p f_m \frac{k_p - k_p}{k_p f_p + k_m f_m + \dfrac{3k_p k_m}{4G_m}} \tag{5}$$

where G_m is the shear modulus of matrix.

The measured and calculated results of linear thermal expansion curves for Cu–SiC_p composite are presented in Figure 11. The results show that the CTE decreases as the SiC_p weight fraction increases. The experimental CTEs are much higher than these predictions. The results reflect the weak bonding between SiC_p and Cu, which provides little constraint on the expansion or contraction of the copper matrix.

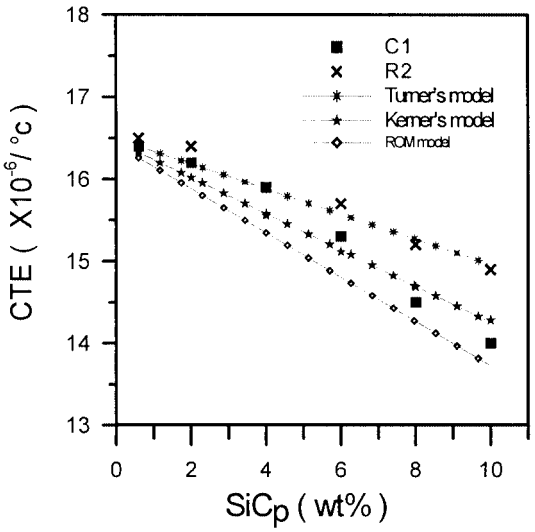

Figure 11. Measured and predicted linear thermal expansion of the Cu–SiC_p composites (200–500°C).

3.8 Material Removal Rates on EDM

Metal removal rate is an important parameter for evaluating the machining performance of EDM for a particular working setup, and the machining rate depends on the electrode manufacturing variable. Material removal rate can be expressed as follows (33):

$$W_m = K_m \cdot \tau_{on}^a \cdot I_p^b \cdot \frac{10^6}{\tau_{on} + \tau_{off}} \tag{6}$$

where W_m is the material removal rate (mm^3/min); K_m, a, and b are coefficients to be determined by test condition; and τ_{on} and τ_{off} (in μsec) are pulse on time and pulse off time, respectively.

A higher discharge current leads to higher discharge energy and energy density. Thus, more material can be melted which increases the removal rate. Figure 12 shows that the material removal rate increases with an increase in applied current. In general, the removal rate varies very little under the normal condition of pulse off time. The pulse on time is taken to be 150 μsec in this research, so the material removal rate increases with the increase of applied current. The maximum removal rate was found for Cu–2wt% SiC$_p$ composite. This suggests that EDM with 2 wt% SiC$_p$ of copper electrode is the better choice for cutting mold steel when pulse time is 150 μsec.

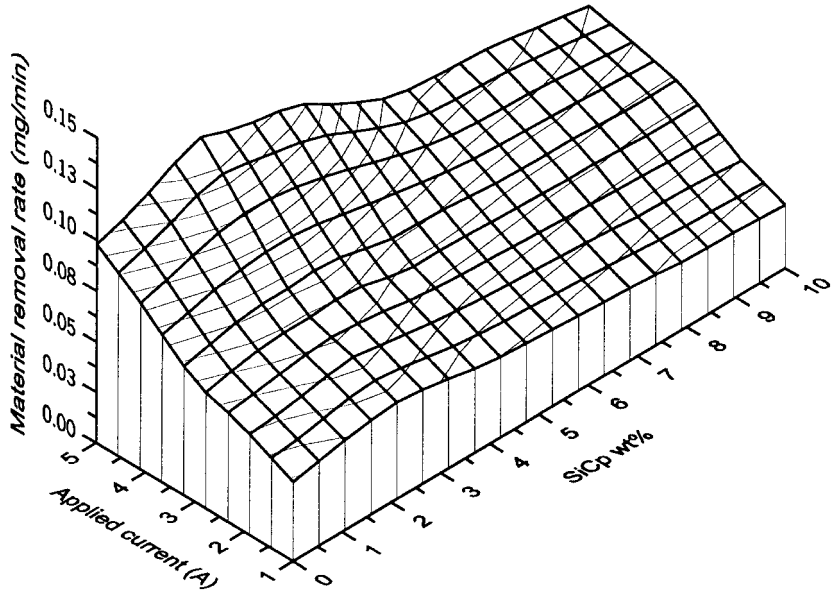

Figure 12. Relationship of the material removal rate, applied current, and SiC$_p$ wt%. (τ_{on} = 150 μsec; τ_{off} = 150 μsec; positive electrode; SKD61 workpiece.)

Table 5. The Product of λ and T_m

Material	Fusion Temperature T_m (K)	Thermal Conductivity $\lambda(w/mk) \times 10^4$	$\lambda \times T_m(w/m)$
Cu	1357	369	40.0
SiC_p	2473	67	14.7

3.9 Electrode Wear Ratio

An ideal EDM tool electrode is the one that not only can remove a large amount of material from the workpiece, but also is capable of resisting self-erosion.

Table 5 shows the fusion temperature and thermal conductivity (λ) for Cu and SiC_p. The electrode wear is roughly proportional to the product of thermal conductivity (λ) and fusion temperature (T_m) (34). Although the fusion temperature of SiC_p is high, because its thermal conductivity is very small, the product of thermal conductivity and fusion temperature ($\lambda \times T_m$) for SiC_p is less than that for Cu, so the ($\lambda \times T_m$) values for the composite are decreased by increasing SiC_p wt%.

The electrode wear P is affected by the discharge pulse energy, which is determined by discharge current and pulse on time, as shown in the following formula (32):

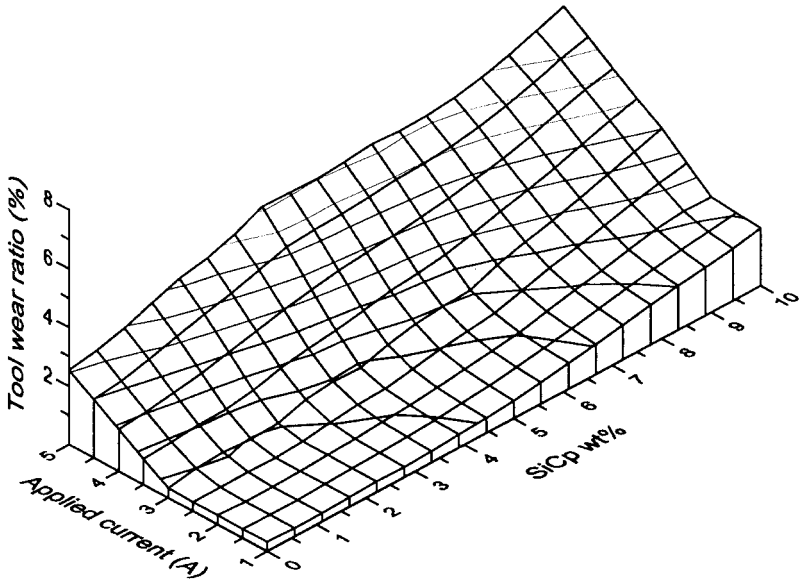

Figure 13. Relationship of the tool wear ratio, applied current, and SiC_p wt% (τ_{on} = 150 μsec; τ_{off} = 150 μsec; positive electrode; SKD61 workpiece.)

$$P = \int_0^{\tau_{on}} u(t)\mathrm{d}t \tag{7}$$

where $u(t)$ is the discharge voltage in V; $i(t)$ is the discharge current in A; and τ_{on} is the pulse on time in μsec. This formula indicates that the increase of discharge current and pulse on time increases the discharge pulse energy as well as the electrode wear.

The variations of tool wear ratio of the electrode with various SiC_p wt% operating at different currents are shown in Figure 13. In general, the tool wear ratio is proportional to the applied current. As discussed above, the higher discharge current leads to higher energy, thus both the material removal rate and tool wear ratio are increased. It also can be observed that the tool wear ratios are almost the same when SiC_p contents are under 4 wt%, and they increase dramatically when SiC_p contents are larger than this value. The $\lambda \times T_m$ value of composite was decreased by increasing SiC_p contents, leading to increased wear ratio with increasing SiC_p contents.

4.0 CONCLUSIONS

The mechanical properties of Cu/SiC_p metal–matrix composite, made by powder sintering and extrusion, can evidently be improved from the pure copper counterpart. This is due to the strengthening effect of SiC powder dispersed into the Cu matrix. It was found that an improved bonding could be achieved by activation of SiC powder surface through electroless coating of Cu onto SiC powder.

From the results of the present work, it was found that a continuous copper film coated on SiC_p by electroless copper coating to form a uniform distribution of SiC_p in Cu matrix is possible. A lower electrode wear ratio can be achieved for EDM testing, and the 2 wt% SiC_p of copper electrode is the better choice for cutting mold steel when pulse time is 150 μsec.

5.0 ACKNOWLEDGMENTS

The authors thank the National Science Council of the Republic of China for the financial support under Grant NSC86-2216-E-009-016 for the experimental aspect of the study. Special thanks are acknowledged to one of the reviewers, who reviewed carefully and made many valuable suggestions on the paper.

6.0 REFERENCES

1. Her, M.G.; Weng, F.T. Int. J. Adv. Manuf. Technol. **2001**, *17*, 715.
2. Marafona, J.; Wykes, C. Int. J. Mach. Tools Manuf. **2000**, *40*, 153.
3. Chen, Y.; Mahdavian, S.M. Wear **1999**, *236*, 350.

4. Park J.; Keller, S.; Carman, G.P.; Hahn, H.T. Sens. Actu. A: Phys. **2001**, *90*, 191.
5. Samuel, M.P.; Philip, P.K. Int. J. Mach. Tools Manuf. **1997**, *37* (11), 1625.
6. German, R.M.; Hens, K.F.; Johnson, J.L. Int. J. Powder Metall. **1994**, *30* (2), 205.
7. Kenny, F.E.; Balbahadur, A.C.; Lashmore, D.S. Wear **1997**, *203*, 715.
8. Hart, R.R.; Wonsiewicz, B.C.; Chin, B.Y. Metall. Trans. **1970**, *1*, 3163.
9. Warrier, K.G.K.; Rohatgi, P.K. Powder Metall. **1986**, *29*, 65.
10. Chang, S.Y.; Lin, S.J. Scripta Mater. **1996**, *35*, 225.
11. Zhang, J.; Laird, C. Acta Mater. **1999**, *47*, 3811.
12. Mortensen, A.; Pedersen, O.B.; Lilholt, H. Scripta Mater. **1998**, *38*, 1109.
13. Jahazi, M.; Jalilian, F. Composites Sci. Technol. **1999**, *59*, 1969.
14. Chang, Y.S.; Lin, S.J. Scripta Mater. **1996**, *35* (2), 225.
15. Zwisky, K.M.; Grant, N.J. Metal Prog. **1961**, *August*, 209.
16. Denisenko, E.T.; Polushko, A.; Filatova, N.A. Porosh Kovaya Metall. **1971**, *10*, 49.
17. Surappa, M.K.; Rohatgi, P.K. Metal. Technol. **1978**, *5* (10), 358.
18. Grimes, J.H.; Scott, K.T.B. Powder Metall. **1968** *11* (22), 213.
19. Rogers J. A.; Miles, D.E.; Hopkins, B.E. Powder Metal. **1973**, *16*, 66.
20. Kobayashi, K.F.; Tachibana, N.; Shingu, P.H. J. Mater. Sci. **1990**, *25*, 3149.
21. Hanada, K.; Murakoshi, Y.; Negishi, H.; Sano, T. *Proceedings of the 45th Japanese Joint Conference for the Technology of Plasticity*, 1994; 760.
22. Groza, J.R.; Gibeling, J.C. Mater. Sci. Eng. **1993**, *A171*, 115.
23. Warren, R.; Anderson, C.H. Composites **1984**, *15*, 101.
24. Qin, C.D.; Derby, B. Br. Ceram. Trans. J. **1991**, *90*, 124.
25. Yih, P.; Chung, D.D.L. J. Mater. Sci. **1999**, *34*, 359.
26. Kovacik, J.; Scripta Mater. **1998**, *39* (2), 153.
27. Landauer, R. AIP Conference Proceedings 40, New York, 1978; 2.
28. Beer, F.P.; Johnston, E.R. *Mechanical Behavior of Materials*, 2nd Ed.; McGraw-Hill: New York, 1996; 806.
29. Courtney, T.H. *Mechanical Behavior of Materials*, 2nd Ed.; McGraw-Hill: New York, 1996; 46.
30. *ASM Handbook*, Vol. 2; American Society for Metals: Metals Park, OH, 1991; 401.
31. Sun, Q.; Inal, O.T. Mater. Sci. Eng. **1996**, *B41*, 261.
32. Turner, P.S.; J. Res. Nat. Bur. Stand. **1946**, *37*, 239.
33. Zhang, J.H.; Lee, T.C.; Lau, W.S. J. Mater. Proc. Technol. **1997**, *63*, 908.
34. Kerner, E.H. Proc. Phys. Soc. **1956**, *B69*, 808.

MARCEL DEKKER, INC.
270 Madison Avenue, New York, New York 10016